Flow Turbulence Combust (2013) 91:451–473
DOI 10.1007/s10494-013-9502-8

From Streaks to Spots and on to Turbulence: Exploring the Dynamics of Boundary Layer Transition

Tamer A. Zaki

Received: 1 January 2013 / Accepted: 27 July 2013 / Published online: 18 September 2013

> "...an eerie type of chaos can lurk just behind a facade of order, and yet deep inside the chaos lurks an even eerier type of order." Douglas Hofstadter

Abstract Bypass transition to turbulence in boundary layers is examined using linear theory and direct numerical simulations (DNS). First, the penetration of low-frequency free-stream disturbances into the boundary layer is explained using a model problem with two time scales, namely the shear and wall-normal diffusion. The simple model provides a physical understanding of the phenomenon of shear sheltering. The second stage in bypass transition is the amplification of streaks. Streak detection and tracking algorithms were applied to examine the characteristics of the streak population inside the boundary layer, beneath free-stream turbulence. It is demonstrated that simple statistical averaging masks the wealth of streak amplitudes in transitional flows, and in particular the high-amplitude, relatively rare events that precede the onset of turbulence. The third stage of the transition process, namely the secondary instability of streaks, is examined using secondary instability analysis. It is demonstrated that two types of instability are possible: An outer instability arises near the edge of the boundary layer on the lifted, low-speed streaks. An inner instability also exists, and has the appearance of a near-wall wavepacket. The stability theory is robust, and can predict the particular streaks which are likely to undergo secondary instability and break down in transitional boundary layers beneath free-stream turbulence. Beyond the secondary instability, turbulent spots are tracked in DNS in order to examine their characteristics in the subsequent non-linear stages of transition. At every stage, we compare the findings from linear theory to the empirical observations from direct solutions of the Navier-Stokes equations. The complementarity between the theoretical predictions and the computational

T. A. Zaki (✉)
Department of Mechanical Engineering, Imperial College London, London SW7 2AZ, UK
e-mail: t.zaki@imperial.ac.uk

experiments is highlighted, and it leads to a detailed view of the mechanics of transition.

Keywords Boundary layers · Transition to turbulence · Bypass transition · Streaks · Turbulent spots

1 Introduction

Fluid dynamicists have long marvelled at the inception of turbulence and the emergence of its whirls and eddies from orderly fluid motion. This keen interest in transition to turbulence has inspired a wealth of research activities into its various forms, in single- and two-phase flows and in simple and complex fluids. In addition to the interest in its fundamental aspects, transition has important practical implications due to the enhanced mixing of momentum, higher skin-friction drag and heat transfer rates associated with the onset of turbulence.

The route to turbulence is not unique, even within a single flow configuration. For instance, in boundary layers, transition can take place via Tollmien–Schlichting instability waves [22], cross-flow instabilities [36], or Görtler instabilities [13, 38] among a wealth of other mechanisms. In an engineering flow configuration, for example a compressor or turbine passage (see Fig. 1), transition can be due to leading-edge effects [30, 33], curvature [38], the pressure distribution along the blade surface [44] or migrating disturbances from upstream stages [42, 46]. Efforts to understand the relevance of various flow configurations have focussed on canonical problems, in order to isolate a particular effect. However, a confluence of various mechanisms is also possible, and can lead to new transition phenomena [25, 26].

We herein focus on zero-pressure-gradient boundary layers, where transition to turbulence is usually classified as orderly or bypass. The orderly transition process is well defined: It starts with the amplification of discrete Tollmien–Schlichting instability waves, followed by their secondary instability and finally breakdown to

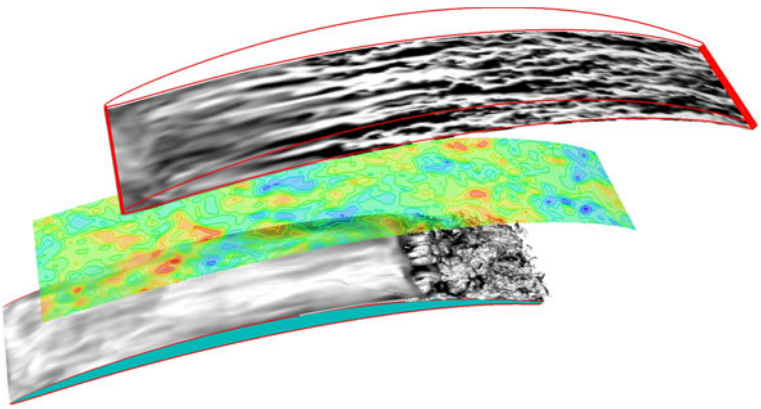

Fig. 1 Transition to turbulence in a compressor passage due to migrating free-stream turbulence [47]. *Gray contours* show the tangential velocity perturbation, u_t', near the blade surface, $-0.12 < u_t' < 0.12$ The pressure surface boundary layer undergoes bypass transition. The suction surface boundary layer undergoes laminar separation and turbulent reattachment

turbulence. The term bypass, on the other hand, has been used to refer to all other routes which lead to boundary layer turbulence, but deviate from the orderly scenario. The simple terminology singled out the orderly transition process, which reflects the focus of the original research efforts on that path. More recently, the term bypass started to become synonymous with one breakdown scenario, when boundary layers are exposed to free-stream vortical forcing. It is this form of breakdown that is the focus of the current review.

1.1 Bypass transition

When laminar boundary layers are exposed to free-stream vortical disturbances, they undergo transition to turbulence in an intriguing manner—see the pressure surface of the blade in Fig. 1. Despite the broadband nature of the free-stream forcing, the boundary layer is only distorted by low-frequency disturbances. This filtering process is known as shear-sheltering, a term coined by Hunt and Durbin [19] in reference to the ability of the shear to filter high-frequency vortical disturbances. Inside the boundary layer, the elongated distortions reach high amplitude, which can be larger than 10 % of the mean flow speed when the free-stream turbulence-intensity is only 3 %. These distortions are termed Klebanoff modes and have been studied using linear theory [e.g. 18, 27, 43], experiments [e.g. 29, 41] and using direct numerical simulations [2, 43]. The final stage is the secondary instability of particular streaks, which precedes breakdown into turbulent spots. Secondary instability analyses were invoked in order to explain the possible modes of breakdown [e.g. 2, 40]. Beyond the secondary instability of streaks, turbulent spots are formed and spread as they convect downstream. Their sporadic onset, growth and merging maintains the downstream edge of the fully-turbulent boundary layer.

The development of Klebanoff modes has received great attention in the literature on bypass transition. An explanation of the mechanism for the amplification of streaks was provided by rapid distortion theory [34]. A physical interpretation in terms of vertical displacement, or lift-up, of mean momentum was provided by Landahl [23]. The details of their amplification beneath free-stream turbulence have been studied experimentally [28, 29], using direct numerical simulations [21] and theory [12, 24]. Some of the literature has focused on the linearly-optimal streaks, which would arise due to an upstream optimal disturbance. While such a disturbance might not be present in the flow, the analysis correctly predicts the width of the streaks observed in experiments and their downstream amplification [1].

The connection between Klebanoff modes and breakdown to turbulence is less clear, and has often been sought based on evidence from DNS [e.g. 21, 37] and experiments [e.g. 31]. The DNS by Jacobs and Durbin [21] showed that the low-speed streaks can become unstable when they are lifted towards the edge of the boundary layer where they are exposed to free-stream forcing by high-frequency modes. Zaki and Durbin [43] examined this transition mechanism using simulations of the interaction between only two free-stream vortical modes: A low-frequency disturbance which penetrates the shear and generates amplifying streaks. The second, high-frequency vortical mode remains in the free stream due to shear sheltering. However, it forces the lifted low-speed streaks at the edge of the boundary layer, and causes their secondary instability and bypass transition to turbulence. These simulations provided an uncluttered view of the essential interaction that precedes breakdown.

The same methodology was used to explore the effects of pressure gradients [44] and the interaction between streaks and discrete instability waves [8, 25, 26].

The empirical observations from DNS and experiments motivated theoretical studies of the instability of streaky boundary layers. In analogy to the work by Swearingen and Blackwelder [39] on the secondary instability of Görtler flows, Andersson et al. [2] performed secondary instability analyses of linearly-optimal streaks. They found that streaks must reach a very high amplitude, on the order of 26 %, in order to develop the first unstable mode. This value is much higher than expected from experiments and simulations. As will be demonstrated herein, streaks with such high amplitude often host turbulent spots—an indication that the instability is mature, and was initiated much earlier when the streaks were at lower amplitudes.

Another unanswered question regarding the stability of streaks was raised by the work of Nagarajan et al. [30]. They showed that transition is not only initiated near the edge of the boundary layer, but can also be initiated near the wall, in the form of wave-packets. This was the case in their simulations of zero-pressure-gradient boundary layers when the leading edge was blunt. The role of the Klebanoff distortions in this case is less clear. The stability analysis by Vaughan and Zaki [40] provided an explanation, and will be discussed herein.

Beyond streak instability, the formation of turbulent spots and their growth to form the fully-turbulent boundary layer has also been of interest since the work of Emmons [10]. It is difficult to study naturally occurring spots in experiments due to their sporadic onset in space and time. Therefore, experiments have resorted to artificially triggering turbulent spots, for example using a disturbance at the wall [7], and studying their evolution. On the other hand, direct numerical simulations provide a unique facility to investigate in detail naturally occurring spots in simulations of bypass transition beneath free-stream turbulence. By storing time-series of the flow field and applying laminar–turbulent discrimination, it is possible to identify these turbulent regions and to characterise their growth mechanism and rate.

The structure of this paper follows the proceedings of bypass transition. After a brief description of the governing equations and the solution techniques, we discuss the following three stages. First, the low-pass filtering ability of the shear is discussed using a model problem, in order to explain shear-sheltering and the penetration of low-frequency disturbances into the boundary layer. Second, we characterise the population of streaks which grow inside the shear. Finally, we address the secondary instability of streaks. Throughout the presentation, we refer to our group's recent research activity in each of these areas—an activity that relies on direct numerical simulations (DNS) and linear theory. We draw on the results of linear theory to interpret empirical observation from numerical simulations, and new observations from DNS motivate more advanced theory. This complementarity has proven essential in developing a clear understanding of the proceedings of bypass transition.

2 Governing Equations

Throughout our discussion of bypass transition, we will refer to observations from Direct Numerical Simulations (DNS) of the full Navier-Stokes equations and results from linear theory. Both frameworks are introduced briefly in this section, and the

focus is directed towards the deductions based on these methods, rather than the details of their solution.

2.1 Direct numerical simulations

Direct numerical simulations of bypass transition are largely possible due to the moderate Reynolds number, and therefore the ability to accurately resolve all flow scales by solving the full Navier-Stokes equations. The governing equations are therefore the incompressibility constraint, and the Navier-Stokes equations,

$$\frac{\partial u_i}{\partial x_i} = 0 \tag{1}$$

$$\frac{\partial u_i}{\partial t} + u_j \frac{\partial u_i}{\partial x_j} = \frac{\partial p}{\partial x_i} + \frac{1}{R} \frac{\partial^2 u_i}{\partial x_j \partial x_j}, \tag{2}$$

where $u_i = \{u, v, w\}$ is the velocity vector, p is the pressure, and R is the Reynolds number. In the following, uppercase variables and overline denote mean flow quantities (e.g. $\overline{U}$ which are obtained by spanwise and time-averaging, and primed variables represent perturbation quantities (e.g. u'). The Navier-Stokes equations are solved using a fractional-step procedure. The equations are discretised on a curvilinear, staggered grid using local volume fluxes. The convective terms are treated explicitly using Adams-Bashforth; the pressure and diffusive terms are advanced implicitly using Euler and Crank-Nicolson schemes, respectively. Details of the numerical method are given in the work of Rosenfeld et al. [35], and examples of its use in transition prediction include simulations of transition in pressure gradients [44], breakdown to turbulence due to Görtler instability [38], and transition in complex geometries [47].

Results presented herein are from simulations of zero-pressure-gradient boundary layers undergoing bypass transition beneath free-stream turbulence. The schematic of the computational domain is shown in Fig. 2. The setup is similar to the original work of Jacobs and Durbin [21], where the inlet to the computational domain is downstream of the leading edge, and the inflow is a superposition of the Blasius profile and free-stream turbulence. The turbulence is synthesised from Fourier modes in the periodic spanwise direction and in time, and is a superposition of eigenmodes of the linear perturbation equations in the wall-normal direction as first introduced by Jacobs and Durbin [21]. The same approach has since been used by

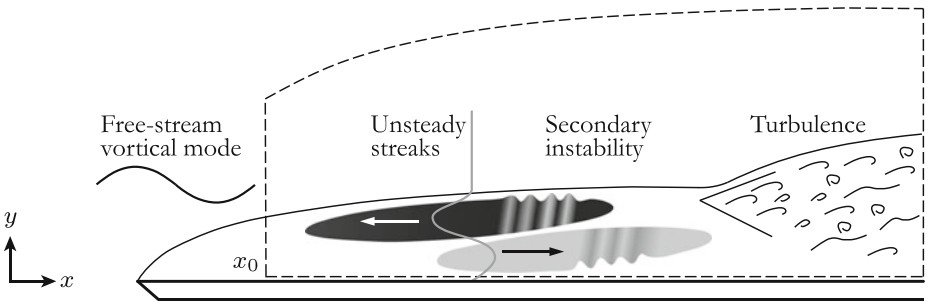

Fig. 2 Schematic of streaky boundary layer response to free-stream forcing, secondary instability and onset of turbulence

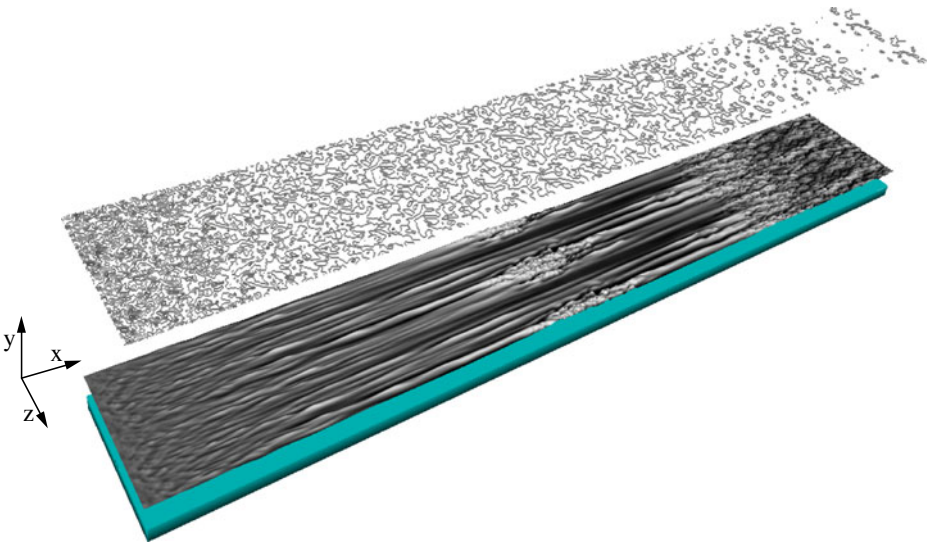

Fig. 3 Boundary layer breakdown beneath free-stream turbulence. Contours of the streamwise velocity perturbation, $-0.15 < u' < 0.15$, at two planes: inside the boundary layer and in the free stream. Turbulent spots and the fully-turbulent boundary layer downstream are shown

a number of researchers [e.g. 4, 32]. At the inlet to the domain, the turbulence intensity is $Tu = 3$ %, and the Reynolds number is $R \equiv U_\infty \delta_0/\nu = 800$ based on the characteristic velocity, U_∞, and 99 % boundary layer thickness $\delta_0 = \delta(x = x_0)$. The no-slip condition is applied at the wall, and the top boundary, which is a free-stream surface, is contoured to ensure zero-pressure-gradient in the streamwise direction. A convective boundary condition is applied at the exit plane.

Both statistics and time-series of the velocity field were extracted from the DNS and will be used throughout the discussion. The database of the velocity fields includes 4000 snapshots of the velocity vector, at every-other grid point of the field, and separated by two time units, based on the convective timescale. An example of the perturbation field is shown in Fig. 3. The two planes shown correspond to a wall-normal location inside the shear and in the free stream. The snapshot contrasts the perturbation fields at the two heights, and highlights the formation of elongated, high-amplitude streaks inside the boundary layer, and the formation of turbulent spots which ultimately spread and become the fully-turbulent boundary layer downstream.

2.2 Linear theory: the Orr–Sommerfeld and Squire equations

The evolution of a small perturbation in a parallel shear flow is governed by the Orr–Sommerfeld and Squire equations for wall-normal velocity, v', and vorticity, η', respectively. Assuming a base state $U(y)$, these equations are,

$$\partial_t \begin{bmatrix} v' \\ \eta' \end{bmatrix} = \begin{bmatrix} \Delta^{-1}\left\{d_y^2 U \partial_x + \left(R^{-1}\Delta - U\partial_x\right)\Delta\right\} & 0 \\ -d_y U \partial_z & R^{-1}\Delta - U\partial_x \end{bmatrix} \begin{bmatrix} v' \\ \eta' \end{bmatrix} \tag{3}$$

where Δ is the Laplacian operator, and Δ^{-1} is its formal inverse. The initial-value-problem (3) can be solved for the evolution of v' and η' [see e.g. 43].

The eigenvalue problem associated with Eq. 3 above can be obtained by assuming a Fourier representation in the homogeneous streamwise and spanwise directions and in time,

$$\begin{bmatrix} v'(\mathbf{x},t) \\ \eta'(\mathbf{x},t) \end{bmatrix} = \begin{bmatrix} \phi(y) \\ \chi(y) \end{bmatrix} e^{i(k_x x + k_z z - \omega t)}.$$

The resulting eigenvalue problem is,

$$-i\omega \begin{bmatrix} \phi(y) \\ \chi(y) \end{bmatrix} = \begin{bmatrix} \mathcal{L} & 0 \\ -\mathcal{C} & \mathcal{S} \end{bmatrix} \begin{bmatrix} \phi(y) \\ \chi(y) \end{bmatrix} \tag{4}$$

where

$$\mathcal{L} = \Delta^{-1}\left\{ik_x U'' + \left[\Delta(\Delta)/R\right] - ik_x U\Delta\right\},$$
$$\mathcal{S} = \left[(\Delta/R) - ik_x U\right],$$
$$\mathcal{C} = ik_z U'.$$

For semi-bounded domains, the eigenspectrum of the Orr–Sommerfeld and Squire equations includes a discrete set of eigenvalues ω_n, $n = 1, 2, 3 \ldots N$, whose eigenfunctions vanish in the free stream, $\lim_{y\to\infty} \phi_n, \chi_n(y) = 0$. The eigenspectrum also includes a continuous branch of modes with eigenvalues ω_{k_y} where k_y is a parameter. Eigenmodes which belong to the continuous branch are bounded in the free stream, $\lim_{y\to\infty} \phi_{k_y}, \chi_{k_y}(y)$ bounded. Outside the boundary layer, these eigenfunctions resemble Fourier modes with wall-normal wavenumber k_y. Inside the boundary layer, they decay towards the wall [15].

3 Shear Sheltering

In bypass transition, the disturbance environment in the free stream and inside the boundary layer are starkly different. The turbulence in the free stream is largely defined by its upstream properties, e.g. with respect to homogeneity and isotropy, and decays as it is convected downstream. Inside the boundary layer, the disturbance field is dominated by low-frequency streaks, which are the boundary layer response to the broadband forcing from the free stream. Figure 3 suggests a filtering process whereby only the low-frequency components of the free-stream turbulence penetrate the boundary-layer shear and lead to the formation of streaks. This phenomenon is known as "shear sheltering" [19], and was investigated by Jacobs and Durbin [20] and Zaki and Saha [45]. A physical interpretation of the sheltering behaviour of the shear is given herein, after the work of Zaki and Saha [45].

The basic mechanism for sheltering is based on the relationship between two timescales: the timescale associated with the convection of a wave relative to an observer inside the shear, and the timescale of wall-normal diffusion into the boundary layer. This relationship can be explained with the aid of the schematic in Fig. 4, which elucidates the difference between low- and high-frequency disturbances, and the propensity of the former to penetrate the shear.

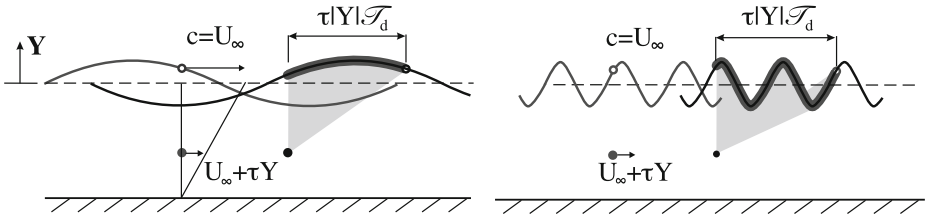

Fig. 4 Schematic of modal penetration for low- and high-frequency free-stream vortical perturbations

Consider a free-stream disturbance which convects at the free-stream velocity, U_∞. An observer inside the shear is traveling at a lower speed, $U_\infty + \tau Y$ where τ is the mean shear and $Y < 0$ is inside the boundary layer. The relative speed is therefore $\tau|Y|$. The influence of the free-stream disturbance reaches the observer over a diffusion timescale, $\mathscr{T}_d \equiv 1/k_y^2\nu$, where k_y is the wall-normal wavenumber of the disturbance (not shown in the schematic).

During the characteristic diffusion time, the wave has convected a distance $\tau|Y|\mathscr{T}_d$ relative to the observer. Therefore, the number of wavelength that have streamed past the observer can be computed according to,

$$n = \frac{\tau|Y|\mathscr{T}_d}{1/k_x} = \frac{\tau|Y|/k_y^2\nu}{1/k_x} = \frac{k_x\tau|Y|}{k_y^2\nu}. \tag{5}$$

In the limit of weak shear or very long waves (small k_x), the observer is subject to a quasi-steady free-stream disturbance; this case is shown schematically at left in Fig. 4. In the limit of very high shear or short disturbance wavelength (large k_x), the number of waves that stream past the observer is large. The net effect at the observer location is vanishing since it is the "average" of many waves; this scenario is shown at right in Fig. 4.

Based on the above model, the penetration of free-stream disturbances into the shear is dependent on the ratio of two timescales: wall-normal diffusion $\mathscr{T}_d \equiv 1/\left(k_y^2\nu\right)$ and the shear $\mathscr{T}_s \equiv 1/\left(k_x\tau\delta_{BL}\right)$. When the diffusion time is relatively short, an observer can "resolve" the free-stream disturbance that is convected at a relatively higher speed. Under strong shear, or when the diffusion time is relatively long, the observer cannot "resolve" the free-stream disturbance.

Two observations are important to note as they have important implications on potential control strategies: First, the disturbance that is most effective at penetrating the boundary layer has a horizontal wavenumber vector (k_x, k_z) which is orthogonal to the shear. Here, the horizontal wavenumber is $(k_x = 0, k_z)$ and the shear vector is $(dU/dy, dW/dy) = (\tau, 0)$. Second, the effect of the shear is cumulative: As the distance from the edge of the boundary layer is increased, the value of n also increases. As a result, only progressively lower-frequency waves can penetrate into the boundary layer closer to the wall. Motivated by these observations, Hack and Zaki [16] investigated a control strategy aimed at sheltering the boundary layer from free-stream turbulence by introducing time-dependent shear via wall oscillation. The introduction of a Stokes layer leads to a varying shear angle with wall-normal height. As a result, the sub-spectrum that can permeate the shear changes with proximity

to the wall, and the cumulative filtering effect reduces the fraction of free-stream energy that can penetrate towards the wall.

4 Amplification of Streaks

Once low-frequency disturbances penetrate the boundary layer, they lead to the amplified streaky structures inside the shear. The streaks have a high amplitude of the streamwise velocity perturbation, while the cross-stream perturbations remain relatively weak. Streaks have been the subject of a wealth of investigations: Their elongated streamwise extent and high amplitude are well understood based on linear theory. Rapid distortion theory demonstrates that low-frequency disturbances will continue to amplify, without the action of restoring pressure [9, 34]. These disturbances are, therefore, the preferred boundary layer distortion which will dominate at long time.

An alternative view is provided from the perturbation equations (3), which cover the linear evolution of an initial disturbance in parallel boundary layer flow. Optimisation over all possible initial conditions, in order to obtain the most amplifying linear disturbance, has been performed by Butler and Farrell [6]. They demonstrated that the optimal initial condition is a periodic arrangement of counter-rotating streamwise vortices that lead to the amplification of streaks with wall-normal and spanwise sizes on the order of the boundary layer thickness. Since the Orr–Sommerfeld equation is homogeneous, a small amplitude vertical velocity perturbation, v', will simply decay due to viscous effects at sub-critical Reynolds number. The Squire equation, on the other hand, is forced by the vertical velocity. The response to this Orr–Sommerfeld forcing is an amplification in the normal vorticity, η'. Zaki and Durbin [43] demonstrated that resonance exists between continuous Orr–Sommerfeld modes and the Squire operator. As a result, the Squire response amplifies linearly in time prior to the long-term viscous decay.

Since the streaks reach large amplitudes, linear theory is not sufficient, and non-linear simulations are required in order to accurately predict the evolution of streaks. In addition, beneath free-stream turbulence, a wide spectrum of streaks is observed inside the boundary layer. Previous studies based on direct numerical simulations have, however, reduced the rich spectrum of streaks to simple statistical quantities, e.g. the root mean square velocity disturbance. Nolan and Zaki [32] adopted a different view: They considered the distribution of streak amplitudes within the transitional boundary layer, with the objective of identifying the particular streaks which undergo secondary instability and breakdown to turbulence. First, they applied laminar-turbulence discrimination in order to isolate the non-turbulent region of the flow from DNS fields. Streak tracking was subsequently applied in order to determine the characteristics of the streak population.

An example of laminar-turbulence discrimination is shown in Fig. 5. In order to distinguish between the turbulent and non-turbulent flow, a detector function is required. Here, the disturbance velocity in the cross-flow plane is used, namely $D \equiv |v'| + |w'|$. In the streaky, pre-transitional region, the value of D is small and increases sharply with the onset of turbulent spots. The detector function is first low-pass filtered, and subsequently thresholded to yield an indicator function, Γ, which is a logical indicator of turbulent ($\Gamma = 1$) versus non-turbulent ($\Gamma = 0$) flow.

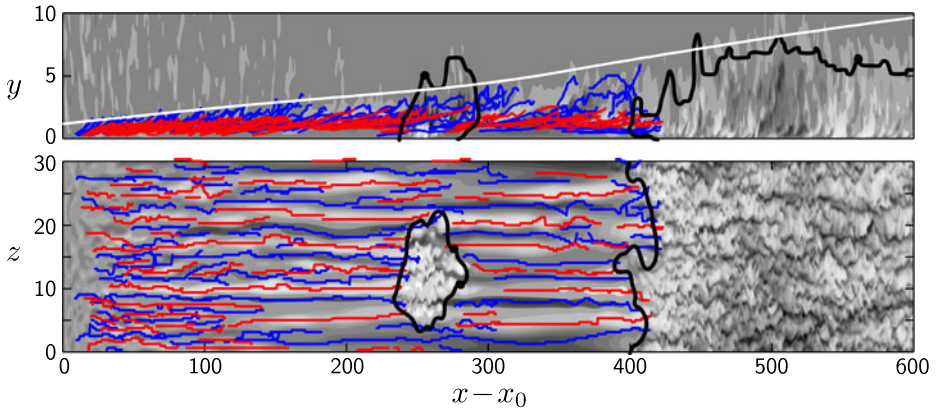

Fig. 5 Side (*top*) and plan (*bottom*) views showing laminar-turbulent discrimination. The *black line* denotes the boundary between the turbulent and non-turbulent flows. Contours are the streamwise velocity perturbation, u', with high- and low- speed streaks marked in *red* and *blue*, respectively

Once the non-turbulent region of the flow is identified, streak detection is performed. Since the streaks are characterised by large u' perturbations, a local maxima identification technique is effective at isolating the core of the streaks at each streamwise location. These maxima are correlated in successive cross-flow planes in order to establish the connectivity of the streaks. An example of the result for streak detection is shown in Fig. 5. The cores of the high- and low-speed streaks are identified in the figure by the blue and red lines, respectively.

The streaks from successive snapshots are cross-correlated in order to construct a time-history of streak evolution. An example of streak evolution in space-time is shown in Fig. 6. The streak is treated as a Lagrangian object, denoted s, in space and

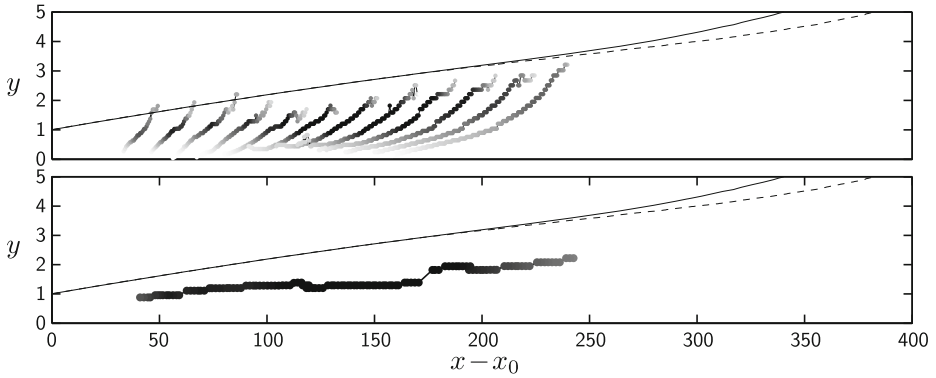

Fig. 6 *Top frame* Side view showing the evolution of a low-speed streak in space and time, as it convects and amplifies downstream. The time interval between two streak instances is twenty time units. Contours are the streak amplitude, $\mathcal{A}_u^s$. *Bottom frame* The wall-normal location, y^s, of the maximum amplitude A_u^s during the streak evolution. The mean (*solid line*) and laminar-conditioned (*dashed line*) boundary-layer edges are also shown

time. The coordinates of its core are therefore a function of time, and are denoted $\mathbf{x}^s(t)$, and the amplitude is defined by,

$$\mathcal{A}_u^s(\mathbf{x}^s, t) \equiv u'(\mathbf{x} = \mathbf{x}^s, t). \tag{6}$$

At every streamwise location, the maximum streak amplitude over its history can be extracted,

$$A_u^s(x) = \max_{t,y,z} \left(\mathcal{A}_u^s(\mathbf{x}^s, t)\right), \tag{7}$$

as well as the wall-normal height of the occurrence of this maximum,

$$y^s(x) = y\left(A_u^s(x)\right). \tag{8}$$

The above procedure is performed for all the streaks identified during the DNS of bypass transition beneath free-stream turbulence. The probability density function (PDF) of streak amplitudes is shown in Fig. 7, where it is contrasted to transitional averaging techniques, e.g. root mean square values. At left, the distribution of A_u is plotted at a particular downstream location from the leading edge. The figure also includes the distribution of u' perturbations in grey, and the root mean square value, u_{rms}, is indicated by the vertical dashed line. It is evident from the figure that the often reported u_{rms} underpredicts the average streak amplitude and, more importantly, the high intensity streaks at the tails of the distribution. The latter are the rare events which lead to the onset of turbulent spots and full non-linear breakdown to turbulence. The right hand pane shows the evolution of the PDF with downstream distance. In addition, the circles on the figure identify the streaks which hosted the inception of turbulent spots. As evident from the figure, streaks with amplitudes, $A_u \geq 0.2$, are the most likely events to initiate breakdown to turbulence. This result would be masked by conventional statistical averaging techniques.

The above discussion has thus far addressed (a) the penetration of low-frequency free-stream disturbances into the boundary layer and (b) the amplification of streaks. The notion of streak breakdown was only mentioned in connection with a critical streak amplitude. However, the secondary instability which causes the streaks to

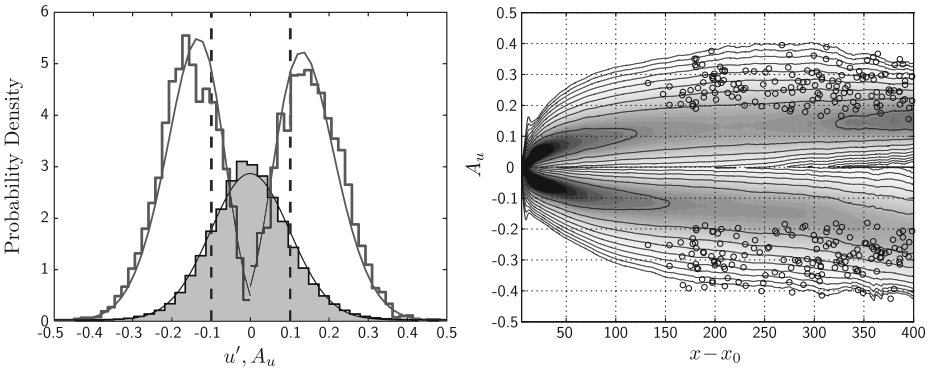

Fig. 7 *Left frame* Probability density function of u' (*grey shading*) and of the streak amplitude. The *vertical line* denotes u_{rms} obtained from time and spanwise averaging of the DNS data. *Right frame* The downstream evolution of the PDF of streak amplitude. *Marked circles* identify the onset of turbulent spots

breakdown to turbulence has not been addressed, and is the subject of the next section.

5 Breakdown to Turbulence

5.1 Secondary instability of idealised streaks

In order to accurately assess the stability of streaky boundary layers, Vaughan and Zaki [40] constructed a database of idealised streaks. These streaks were obtained by forcing the boundary layer with a single inflow continuous Orr–Sommerfeld mode, and computing the emergent streaky flow using DNS. Therefore, the streaks in their analysis take into account non-parallel and non-linear effects. The boundary layer profile was extracted at a target location (see Fig. 2), and secondary instability analysis was performed using Floquet theory. The base flow is therefore a superposition of a boundary layer profile, $U_0(y)$, and a saturated streak $u_1(y, z, t)$,

$$u_2(y, z, t) = U_0(y) + u_1(y, z, t). \tag{9}$$

Since the streaks are periodic in the span and in time, a doubly-periodic Floquet expansion is required. It should also be noted that, while the prescribed free-stream mode is monochromatic in the span and in time, the resulting streaks include harmonics in both dimensions due to non-linear effects. As a result, the Floquet expansion must take into account the various harmonics in the base flow,

$$u_1(y, z, t) = \sum_{m=0}^{M} \sum_{n=0}^{N} \Re\left\{\hat{u}_1^{m,n}(y) e^{i(m\omega t + n k_z z)}\right\}. \tag{10}$$

The velocity profile for a sample streak is shown in Fig. 8. A small mean flow distortion, relative to Blasius, can be seen in the figure and is due to the high-

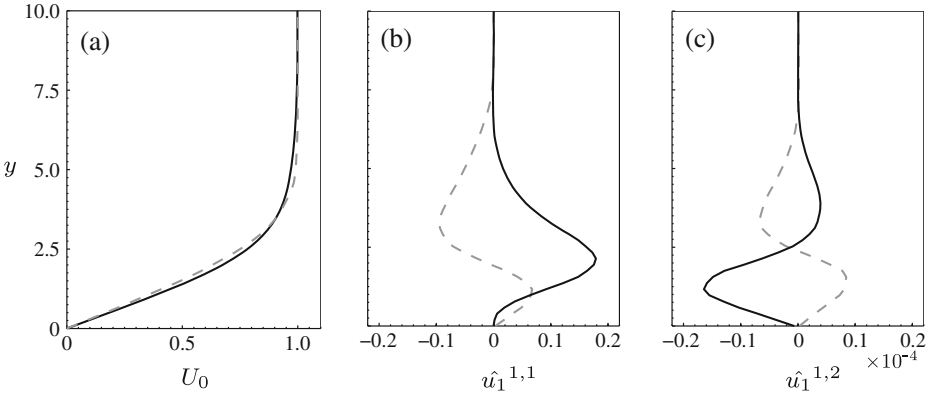

Fig. 8 Wall-normal profile of an example streaky base flow at Reynolds number $R = 360$, streak amplitude $A_u = 20$ % and streak frequency $F = 60$. **a** The distorted mean flow due to the presence of streaks (——) and the Blasius profile (– – –); **b** the fundamental; **c** the spanwise harmonic components (see Eq. 10). In (b,c), *solid* and *dashed lines* are the real and imaginary parts of $\hat{u}_1^{m,n}$

amplitude non-linear streaks. The effect of this distortion is stabilizing, and therefore the streaks must be sufficiently destabilising to lead to overall instability of the base flow.

The linear perturbation equations which govern the evolution of the secondary instability are derived by assuming a total velocity of the form,

$$\boldsymbol{v}(x, y, z, t) = \{U_0(y) + u_1(y, z, t)\}\mathbf{e}_x + B\boldsymbol{v}_3(x, y, z, t), \tag{11}$$

where B is sufficiently small for linearization. Substituting Eq. 11 in the Navier-Stokes equations, the secondary linear instability problem can be expressed in terms of $\nabla^2 v_3$ and η_3, the Laplacian of the wall-normal velocity and the wall-normal vorticity. The continuity equation is also required in order to complete the system,

$$\begin{aligned}
&\frac{\partial^2 U_0}{\partial y^2}\frac{\partial v_3}{\partial x} + \left(\frac{1}{R}\nabla^2 - \frac{\partial}{\partial t} - U_0\frac{\partial}{\partial x} - u_1\frac{\partial}{\partial x}\right)\nabla^2 v_3 \\
&\quad + \left(-\left[\frac{\partial^2 u_1}{\partial y \partial z} + \frac{\partial u_1}{\partial z}\frac{\partial}{\partial y}\right]\eta_3 + \left[\frac{\partial \xi_3}{\partial x} - \frac{\partial \zeta_3}{\partial z}\right]\frac{\partial u_1}{\partial z} \right. \\
&\qquad \left. + \frac{\partial v_3}{\partial x}\left[\frac{\partial^2 u_1}{\partial y^2} - \frac{\partial^2 u_1}{\partial z^2}\right] + \left[\frac{\partial u_3}{\partial z} + \frac{\partial w_3}{\partial x}\right]\frac{\partial^2 u_1}{\partial y \partial z}\right) = 0,
\end{aligned} \tag{12}$$

$$\begin{aligned}
&\left(\frac{1}{R}\nabla^2 - \frac{\partial}{\partial t}\right)\eta_3 - \frac{\partial \eta_3}{\partial x}U_0 - \frac{\partial v_3}{\partial z}\frac{\partial U_0}{\partial y} \\
&\quad - \left(\frac{\partial \eta_3}{\partial x}u_1 + v_3\frac{\partial^2 u_1}{\partial y \partial z} + w_3\frac{\partial^2 u_1}{\partial z^2} - \frac{\partial v_3}{\partial y}\frac{\partial u_1}{\partial z} + \frac{\partial v_3}{\partial z}\frac{\partial u_1}{\partial y}\right) = 0,
\end{aligned} \tag{13}$$

$$\frac{\partial u_3}{\partial x} + \frac{\partial v_3}{\partial y} + \frac{\partial w_3}{\partial z} = 0. \tag{14}$$

The secondary instability $\boldsymbol{v}_3$ is expressed in terms of a Fourier expansion in t and z,

$$\boldsymbol{v}_3 = e^{(i\alpha x + \sigma_r t)} \sum_{m=-\infty}^{\infty} \sum_{n=-\infty}^{\infty} \boldsymbol{v}_{m,n}(y) e^{i([nk_z+\gamma]z + [m\omega + \sigma_i]t)}, \tag{15}$$

where in the temporal problem both α and γ are real parameters, and σ is the complex eigenvalue. The eigenvalue problem governing the secondary instability is obtained by substituting Eq. 15 into Eqs. 12–14.

The growth rates of the two most unstable modes of the boundary layer, when the Klebanoff streaks are steady, are shown in Fig. 9. The results demonstrate the presence of mode competition: Low amplitude streaks render the flow unstable to one type of disturbance; As the streak amplitude is increased, the growth rate of another type of instability becomes dominant. These two modes are referred to as the "inner" and "outer" instabilities, due to the wall-normal location of their respective critical layers. The wall-normal profiles of these two modes are shown in Fig. 10.

In bypass transition under free-stream turbulence, the effect of streak unsteadiness can be important. Therefore, the growth rates of the inner and outer instabilities were evaluated for a range of base-streak frequencies, $F = [0, 60]$. The results are shown in Fig. 11 and demonstrate that, in general, streak unsteadiness increases

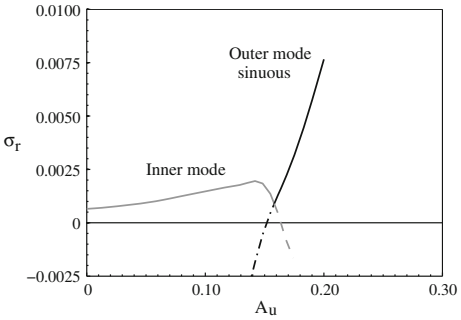

Fig. 9 The growth rate of the two most unstable modes for a boundary layer distorted by steady streaks. The *light line* (——) is the growth rate of the inner mode; the *dark line* (——) is the outer mode

the growth rate of both modes. For the inner mode (Fig. 11a), Vaughan and Zaki [40] showed that the near-wall inflection points in the unsteady base flow play an important role in enhancing instability. They also observed a small stabilizing effect of the inner mode under two conditions: (i) increasing amplitude of steady streaks ($F = 0$), and (ii) increasing frequency at low streak amplitude ($A = 5$ %). These conditions can be related to the literature on steady boundary layer streaks [11, 25, 26] and time-dependent shear flows [14], respectively. Apart from this small stabilizing effect, Fig. 11 establishes that unsteadiness in the base streaks significantly enhances flow instability, be it in terms of the inner or the outer mode.

In order to develop a physical interpretation of these modes, Vaughan and Zaki [40] performed DNS of streaky boundary layers perturbed by an outer or inner instability. The resulting secondary instability of the streaks was computed from the initial linear stages and up to breakdown to turbulence. A top view of the inner instability is shown in Fig. 12 and is contrasted to the wave packets observed by Nagarajan et al. [30]. The spanwise perturbation pattern shows a distinctive checkered pattern near the wall, and which evolves into turbulent spots downstream.

The events which lead to the formation of the turbulent spots are presented in the time sequence in Fig. 13. The inner instability is shown to be most amplified in the

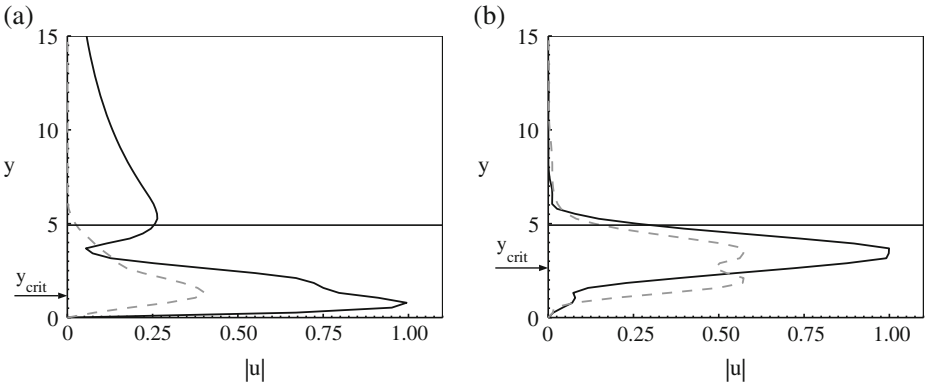

Fig. 10 Wall-normal profiles of **a** the inner and **b** the outer modes. The absolute value of the u−disturbance is plotted for (——) the most energetic and (– – –) the second most energetic components of the Floquet expansion

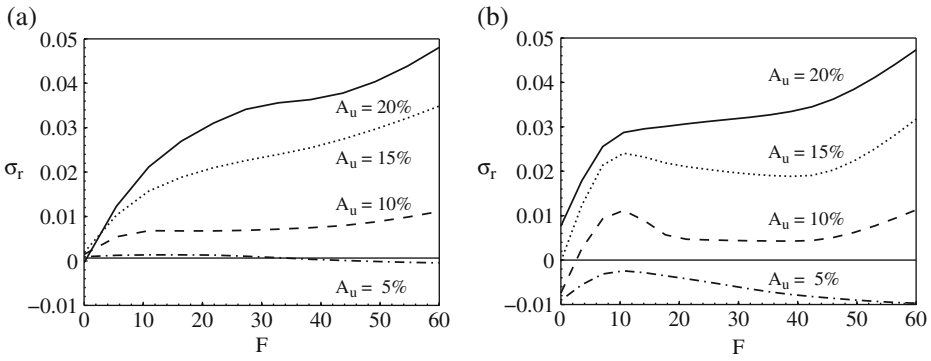

Fig. 11 The influence of streak amplitude and frequency on the **a** inner and **b** outer modes

overlap region between the low- and high-speed streaks. This region has previously been identified as a site of inception of turbulent spots based on empirical evidence only, for example in DNS [5] and experiments [31]. As the inner mode evolves downstream, at later time, the instability intensifies and lifts away from the wall. Ultimately, the secondary instability leads to the formation of turbulent patches and full breakdown to turbulence. It should be noted that the phase speed and growth rate of the inner instability were commensurate with the observations by Nagarajan et al. [30] and much higher than conventional Tollmien–Schlichting waves.

Direct simulations of the outer instability were also performed by Vaughan and Zaki [40]. An overview of the resulting breakdown is shown in Fig. 14. The side view captures the initial laminar streaks, the formation of a turbulent patch and the fully turbulent flow downstream.

The time series which precedes Fig. 14 is shown in Fig. 15. The side views show that the onset of the outer instability is hosted by the lifted, low-speed streaks. These observations are consistent with the breakdown mechanism observed by Jacobs and Durbin [21] in their simulations of bypass transition due to free-stream turbulence. The lifted low-speed streaks are exposed to free-stream turbulence in their simulations, and develop localised instability which lead to breakdown to turbulence. However, the forcing in their simulations was broadband, and the nature of the outer instability was not studied in detail. Here, we have explained the origin on this breakdown in terms of secondary instability analysis and DNS of breakdown due to forcing by the most unstable mode of the base streaks.

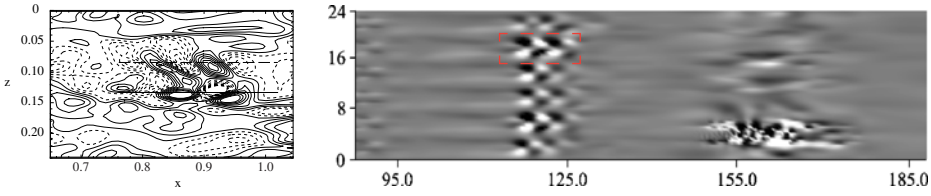

Fig. 12 Top view of the boundary layer. Contours of w' are shown from (*left*) the simulations by Nagarajan et al. [30] and (*right*) the DNS of the inner instability by Vaughan and Zaki [40]

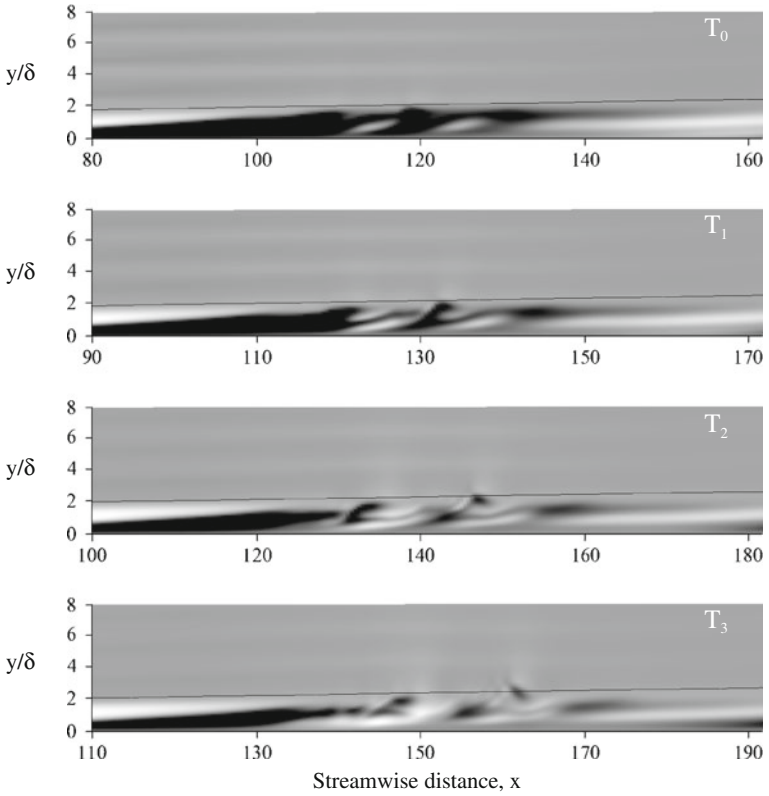

Fig. 13 Time-series showing a side view of the streaky boundary layer response to forcing by an inner instability mode. The contours show streamwise velocity perturbation, u'. The region of the flow-field shown in successive frames is translated downstream in time in order to retain the inner instability in the middle of the viewing window

The existence of an outer and and an inner instability was hypothesized based on empirical observations from the DNS by Jacobs and Durbin [21] and Nagarajan et al. [30], respectively. These observations motivated the Floquet analysis by Vaughan and Zaki [40] which lead to the above findings. Whether an inner or outer instability

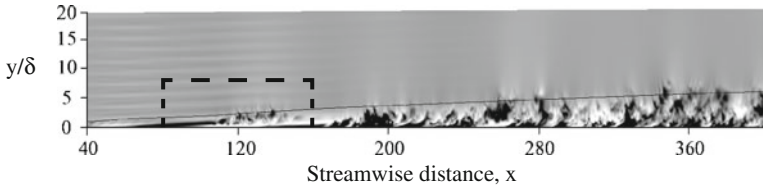

Fig. 14 Side view of the boundary layer when forced by a low-frequency vortical mode to generate streaks and an outer instability wave. The entire domain is shown, contoured with streamwise velocity perturbations, u'

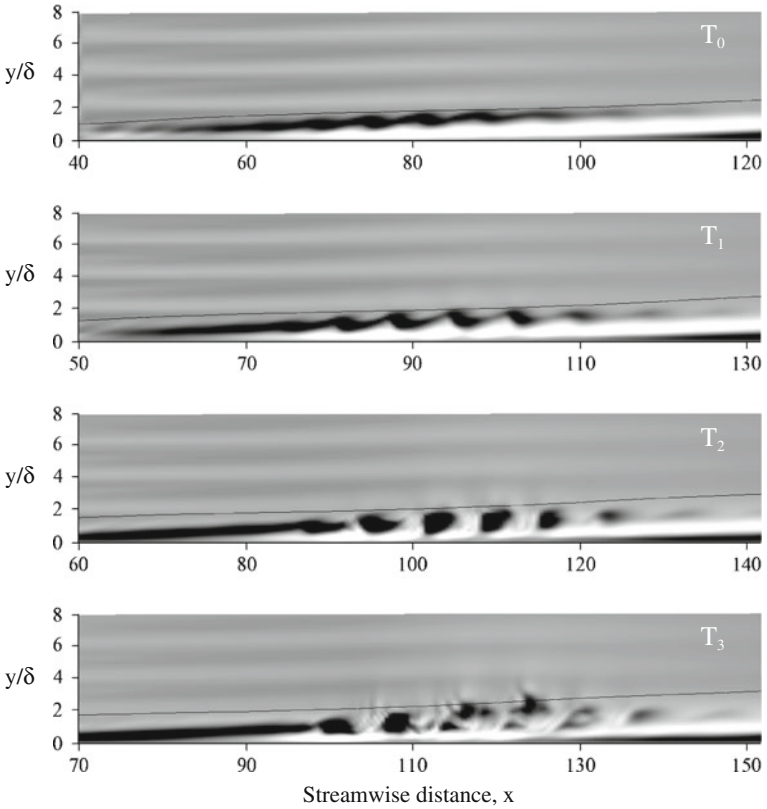

Fig. 15 Time-sequence of the streaky boundary layer in response to inflow forcing by the outer mode. The side view shows the events which precede breakdown to turbulence shown in Fig. 14. The region of the flow-field shown in successive frames is translated downstream in time to maintain the instability in the middle of the viewing window

is observed in a given configuration remains a function of the flow conditions, for example the pressure gradient history and the leading edge geometry.

The study of the secondary instability of idealized streaks presented a significant advance in our understanding of bypass transition. However, a challenging question remained: Can linear stability predict the localised instability of particular streaks in realistic bypass transition under broadband free-stream forcing? These instabilities are localized in space, appear on particular streaks within the boundary layer, and can be of the inner or outer type.

5.2 Secondary instability of realistic streaks

With the encouraging success of linear theory to explain the secondary instability of idealised streaks, Hack and Zaki [17] recently attempted to capture streak instability when the boundary layer is exposed to broadband free-stream turbulence. In this configuration, the flow is laden with streaks, with various spectral content and amplitudes. Examples are shown in Figs. 3, 5 and 16. The challenge is to predict

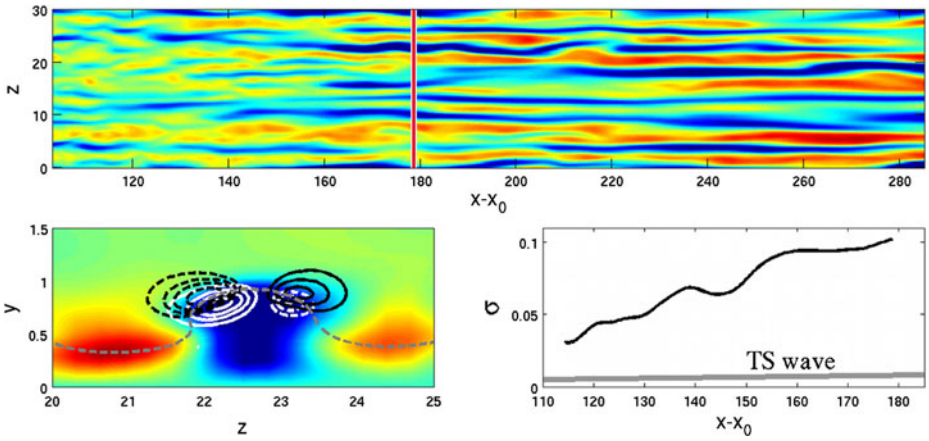

Fig. 16 The secondary instability of streaks beneath free-stream turbulence. *Top pane* Plan view of the streamwise velocity perturbation, u', in the boundary layer. *Bottom pane* At *left*, a zoomed-in end view at $x - x_0 = 178$, focusing on the region where the secondary instability is observed. Contours of the real (*black*) and imaginary (*white*) components of the instability eigenfunction are shown. The *grey line* is the critical layer. At *right*, the growth rate of the instability mode is plotted as the plane of analysis is advanced downstream

which streak, as it evolves downstream, is most unstable and breaks down into a turbulent spot.

Hack and Zaki [17] performed secondary instability analyses for spanwise planes, or two-dimensional base states, which were extracted from the DNS fields. The analysis follows the methodology described in the work of Barkley et al. [3]. The most unstable mode was computed, and its eigenfunction, growth rate and phase speed were recorded. Based on the phase speed, the plane of the analysis was translated downstream at a later time, and the stability analysis was repeated. This procedure was used to track the most unstable mode as it progressed downstream.

The results of the above procedure are presented in Fig. 16 for one streak instability. The top panel shows a plan view of the boundary layer at a time where the low-speed streak has developed a secondary instability near $z = 22.5$. The end view (lower left panel) is a zoomed-in view of the low-speed streak and the secondary instability mode computed from the linear analysis. The magnitude of the instability eigenfunction is marked by the black contour lines, and the critical layer is shown by the dashed line. It is important to remark that the instability eigenfunction is localised on the low-speed streak which subsequently breaks down into a turbulent spot at a later stage. Therefore, the analysis can indeed identify the most unstable streak among the spectrum of Klebanoff distortions, and predict the localised secondary instability of that particular streaks.

The mode shape suggests that this instability is of the outer type. In addition, the wavelength of the instability, as predicted from the linear analysis, compares favourably with the wavelength of the meandering of the streak as observed in the top view. Finally, the growth rate of the instability is also shown at right. The history of the growth rate is plotted from the initial tracking position near $x = 110$ to the final tracking location $x = 180$. It is clear that the growth rate of the mode is much higher than the conventional Tollmien-Schlinchting wave.

In order to determine the statistical relevance of the outer and inner instabilities to the breakdown of boundary layers beneath free-stream turbulence, the above analysis must be repeated for a very long time series. Such effort is currently underway for zero- and adverse-pressure gradient boundary layers. The initial results confirm that the stability analysis is a robust approach to predicting localized streak instability.

5.3 Turbulent spots

Beyond the amplification of streaks and their secondary instability, the formation and growth of turbulent spots was also examined using the laminar-turbulent discrimination techniques presented earlier [32]. An example of spot tracking is shown in Fig. 17. The spot shape is extracted at various downstream locations, from a transitional, adverse-pressure-gradient boundary layer. The silhouette of the spot is coloured by progressively lighter shades to indicate later time instances in the evolution of the turbulent patch. The spread angle is marked in the top view. It is known from previous work that the spread angle depends on pressure gradient, and increases with adverse pressure conditions.

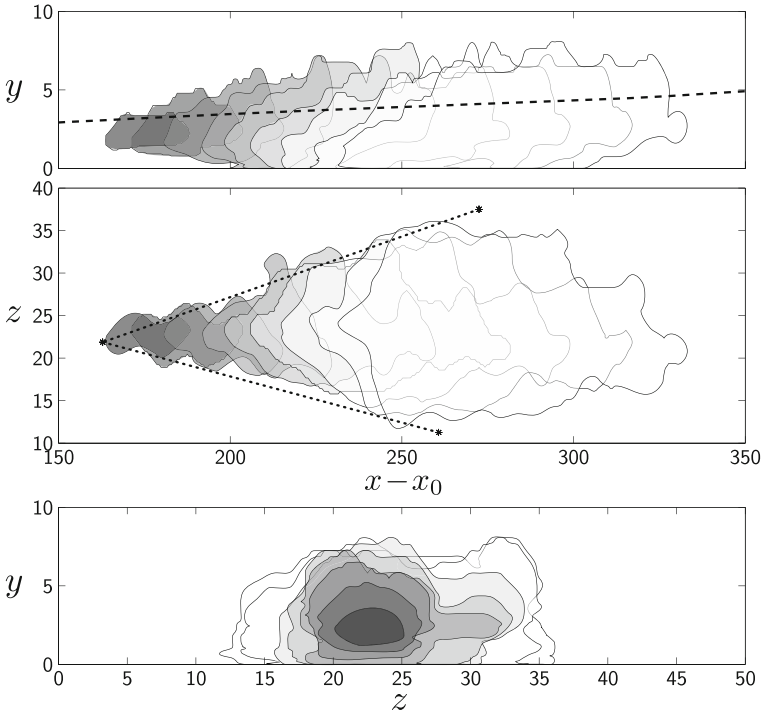

Fig. 17 The history of the growth of a single spot in APG boundary layer. The *spot outline* is shown every 20 convective time units. The *top pane* shows a side view with the laminar-conditioned boundary-layer thickness indicated by a *dashed line*. The *middle* and *bottom* panes show a plan and end view of the spot history

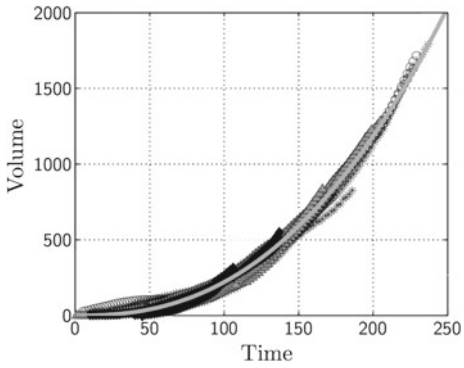

Fig. 18 Spot volume as a function of time extracted from simulations of transition in favourable, zero and adverse pressure gradient boundary layers. Also shown is a power-law fit with an exponent of 2.42

The procedure of spot detection can be repeated for various spots and pressure gradient conditions. Spot characteristics, such as their spreading angle, extent, area and volume can be computed during the evolution of the turbulent patches. The time-dependence of the spot volume for various pressure gradient conditions was evaluated by Nolan and Zaki [32], and is shown in Fig. 18. The volume is independent of the flow conditions, unlike the spreading angle which was the focus of various previous studies. This can be explained in terms of the convective speed of the spots. In adverse pressure gradient, the spots convect at a relatively lower speed, and hence the spread angle increases relative to fast moving spots, for example in favourable pressure gradient. The spot volume, on the other hand, is insensitive to pressure gradient, which could be advantageous for transition modelling.

6 Discussion

Throughout our efforts to explain bypass transition, we have relied on the complementarity between theory and experiments. The theory has often motivated our numerical simulations, and the latter uncovered new phenomena that required the development of more advanced theory. The outcome has been an unprecedented view of the proceedings of transition to turbulence in boundary layers, beneath free-stream vortical forcing.

High-frequency free-stream perturbations are blocked by the boundary-layer shear. In contrast, the ability of low-frequency disturbances to penetrate the shear is evident in experimental and numerical studies of bypass transition. Linear theory of a model problem shed light on the balance between the shear and diffusive time scales, and explained the sheltering effect of the shear.

The propensity of low-frequency distortions to amplify in shear flows is well understood. Therefore, we focused on characterising these streaks in terms of the distributions of their amplitude, when the boundary layer is forced by a broadband spectrum of free-stream vortical modes. The results demonstrate the wealth of streak amplitudes which cannot be inferred by only reporting u_{rms}. The importance of the high-amplitude events, which induce breakdown to turbulence, is demonstrated. These high-amplitude streaks are masked by conventional methods of statistical averaging in the homogeneous flow directions.

The observation of localised breakdown, and its correlation with streak amplitude, motivated a study of the secondary instability of streaks. Doubly periodic Floquet analysis was performed in order to explain the modes of streak instability. Using idealised base streaks, we were able to identify two types of secondary instability: an outer and an inner instability. Both modes can lead to breakdown, and have been used to explain the observations from the numerical experiments by Jacobs and Durbin [21] and Nagarajan et al. [30], respectively. Beyond the stability of idealised streaks, we also demonstrated that linear theory can isolate the most unstable streak, when the boundary layer is exposed to broadband free-stream forcing and is laden with various streaks with different amplitudes. Such predictive capability is unprecedented and is currently being exploited to explore the effects of pressure gradients on boundary layer stability in realistic flow configurations.

The complementarity between theory and simulations has advanced our understanding of every stage of bypass transition to turbulence. This understanding is essential for modelling transitional flows and in the longer term for flow control, for example transition delay. Attempts to target the initial, linear stages of the transition process have aimed at reducing the penetration of vortical disturbances into the shear, and weakening the amplitude of the streak distortions that result. Further efforts in this area will continue to rely on complementarity of theory and experiments, be the latter physical or numerical.

Acknowledgements The author would like to thank Dr. S. Y. Jung, Dr. K. Nolan, Dr. S. Saha, Dr. N. Vaughan, J. Page and P. Hack for their contributions to this research. Financial support was provided by the U.S. Air Force Office of Scientific Research, and the U.K. and the E.U. Research Councils.

References

1. Andersson, P., Berggren, M., Henningson, D.S.: Optimal disturbances and bypass transition in boundary layers. Phys. Fluids **11**(1), 134–150 (1999)
2. Andersson, P., Brandt, L., Bottaro, A., Henningson, D.S.: On the breakdown of boundary layer streaks. J. Fluid Mech. **428**, 29–60 (2001)
3. Barkley, D., Blackburn, H.M., Sherwin, S.J.: Direct optimal growth analysis for time steppers. Int. J. Num. Meth. Fluids **57**, 1435–1458 (2008)
4. Brandt, L., Schlatter P., Henningson, D.S.: Transition in boundary layers subject to free-stream turbulence. J. Fluid Mech. **517**, 167–198 (2004)
5. Brandt, L., de Lange, H.C.: Streak interactions and breakdown in boundary layer flows. Phys. Fluids **20**, 024107 (2008)
6. Butler, K.M., Farrell, B.F.: Three-dimensional optimal disturbances in viscous shear flow. Phys. Fluids A **4**, 1637–1650 (1992)
7. Cantwell, B., Coles, D., Dimotakis, P.: Structure and entrainment in the plane of symmetry of a turbulent spot. J. Fluid Mech. **87**(04), 641–672 (1978)
8. Durbin, P.A., Zaki, T.A., Liu, Y.: Interaction of discrete and continuous boundary layer modes to cause transition. Int. J. Heat Fluid Flow **30**, 403–410 (2009)
9. Durbin, P., Wu, X.: Transition Beneath Vortical Disturbances. Ann. Rev. Fluid Mech. **39**, 107–128 (2007)
10. Emmons, H.W.: The laminar-turbulent transition in a boundary layer. Part i. J. Aero. Sci. **18**, 490–498 (1951)
11. Fasel, H.F.: Numerical investigation of the interaction of the Klebanoff-mode with a Tollmien–Schlichting wave. J. Fluid Mech. **450**, 1–33 (2002)
12. Goldstein, M.E., Wundrow, D.W.: On the environmental realizability of algebraically growing disturbances and their relation to Klebanoff modes. Theor. Comput. Fluid Dyn. **10**, 171–186 (1998)

13. Görtler, H.: Instabilität laminarer Grenzschichten an konkaven Wänden gegenüber gewissen dreidimensionalen Störungen. Z. Angew. Math. Mech. **21**, 250–252 (1941)
14. Grosch, C.E., Salwen, H.: The stability of steady and time-dependent plane Poiseuille flow. J. Fluid Mech. **34**, 177–205 (1968)
15. Grosch, C.E., Salwen, H.: The continuous spectrum of the Orr–Sommerfeld equation. Part 1. The spectrum and the eigenfunctions. J. Fluid Mech. **68**, 33–54 (1978)
16. Hack, M.J.P., Zaki, T.A.: The continuous spectrum of time-harmonic shear layers. Phys. Fluids **24**, 034101 (2012)
17. Hack, M.J.P., Zaki, T.A.: Streak instabilities in boundary layers beneath free-stream turbulence. J. Fluid Mech. (2013, under review)
18. Hultgren, L.S., Gustavsson, L.H.: Algebraic growth of disturbances in a laminar boundary layer. Phys. Fluids **24**, 1000–1004 (1981)
19. Hunt, J.C.R., Durbin, P.A.: Perturbed shear layers. Fluid Dyn. Res. **24**, 375–404 (1999)
20. Jacobs, R.G., Durbin, P.A.: Shear sheltering and the continuous spectrum of the Orr-Sommerfeld equation. Phys. Fluids **10**, 2006–2011 (1998)
21. Jacobs, R.G., Durbin, P.A.: Simulations of bypass transition. J. Fluid Mech. **428**, 185–212 (2001)
22. Kleiser, L., Zang, T.A.: Numerical simulation of transition in wall-bounded shear flows. Ann. Rev. Fluid Mech. **23**, 495–537 (1991)
23. Landahl, M.T.: A note on an algebraic instability of inviscid parallel shear flows. J. Fluid Mech. **98**, 243–251 (1980)
24. Leib, S.J., Wundrow, W., Goldstein, M.e.: Effect of free-stream turbulence and other vortical disturbances on a laminar boundary layer. J. Fluid Mech. **380**, 169–203 (1999)
25. Liu, Y., Zaki, T.A., Durbin, P.A.: Boundary layer transition by interaction of discrete and continuous modes. J. Fluid Mech. **604**, 199–233 (2008)
26. Liu, Y., Zaki, T.A., Durbin, P.A.: Floquet analysis of secondary instability of boundary layers distorted by Klebanoff streaks and Tollmien–Schlichting waves. Phys. Fluids **20**, 124102 (2008)
27. Luchini, P.: Reynolds-number-independent instability of the boundary layer over a flat surface: optimal perturbations. J. Fluid Mech. **404**, 289–309 (2000)
28. Mandal, A.C., Venkatakrishnan, L., Key, J.: A study on boundary-layer transition induced by free-stream turbulence. J. Fluid Mech. **660**, 114–146 (2010)
29. Matsubara, M., Alfredsson, P.: Disturbance growth in boundary layers subjected to free-stream turbulence. J. Fluid Mech. **430**, 149–168 (2001)
30. Nagarajan, S., Lele, S. K., Ferziger, J. H.: Leading-edge effects in bypass transition. J. Fluid Mech. **572**, 471–504 (2007)
31. Nolan, K., Walsh, E.J.: Particle image velocimetry measurements of a transitional boundary layer under free stream turbulence. J. Fluid Mech. **702**, 215–238 (2012)
32. Nolan, K., Zaki, T.A.: Conditional sampling of transitional boundary layers in pressure gradients. J. Fluid Mech. **728**, 306–339 (2013)
33. Ovchinnikov, V., Choudhari, M.M., Piomelli, U.: Numerical simulations of boundary-layer bypass transition due to high-amplitude free-stream turbulence. J. Fluid Mech. **613**, 135–169 (2008)
34. Phillips, O.M.: Shear-flow turbulence. Ann. Rev. Fluid Mech. **1**, 245–264 (1969)
35. Rosenfeld, M., Kwak D., Vinokur M.: A fractional step solution method for the unsteady incompressible Navier-Stokes equations in generalized coordinate systems. J. Comput. Phys. **94**, 102–137 (1991)
36. Saric, W.S., Reed, H.L., White, E.B.: Stability and transition of three-dimensional boundary layers. Ann. Rev. Fluid Mech. **35**, 413–440 (2003)
37. Schlatter, P., Brandt, L., de Lange, H.C., Henningson, D.A.: On streak breakdown in bypass transition. Phys. Fluids **20**, 101505 (2008)
38. Schrader, L.-U., Brandt, L., Zaki, T.A.: Receptivity, instability and breakdown of Görtler flow. J. Fluid Mech. **682**, 362–396 (2011)
39. Swearingen, J.D., Blackwelder, R.F.: The growth and breakdown of streamwise vortices in the presence of a wall. J. Fluid Mech. **182**, 255–290 (1987)
40. Vaughan, N.J., Zaki, T.A.: Stability of zero-pressure-gradient boundary layer distorted by unsteady Klebanoff streaks. J. Fluid Mech. **681**, 116–153 (2011)
41. Westin, K.J.A., Boiko, A.V., Klingmann, B.G.B., Kozlov, V.V., Alfredsson, P.H.: Experiments in a boundary layer subjected to freestream turbulence. Part I: boundary layer structure and receptivity. J. Fluid Mech. **281**, 193–218 (1994)
42. Wu, X., Durbin, P.A.: Evidence of longitudinal vortices evolved from distorted wakes in a turbine passage. J. Fluid Mech. **446**, 199–228 (2001)
43. Zaki, T.A., Durbin, P.A.: Mode interaction and the bypass route to transition. J. Fluid Mech. **531**, 85–111 (2005)

44. Zaki, T.A., Durbin, P.A.: Continuous mode transition and the effects of pressure gradient. J. Fluid Mech. **563**, 357–388 (2006)
45. Zaki, T.A., Saha, S.: On shear sheltering and the structure of vortical modes in single and two-fluid boundary layers. J. Fluid Mech. **626**, 111–148 (2009)
46. Zaki, T.A., Wissink, J.G., Durbin, P.A., Rodi, W.: Direct computations of boundary layers distorted by migrating wakes in a linear compressor cascade. Flow, Turb. & Comb. **83**, 307–322 (2009)
47. Zaki, T.A., Wissink, J.G., Rodi, W., Durbin, P.A.: Direct numerical simulations of transition in a compressor cascade: the influence of free-stream turbulence. J. Fluid Mech. **665**, 57–98 (2010)